

Equivalent Circuit Modeling of the Dielectric Loaded Microwave Biosensor

Muhammad Taha JILANI¹, Wong Peng WEN², Lee Yen CHEONG³, Mohd Azman ZAKARIYA,
Muhammad Zaka Ur REHMAN⁴

¹Dept. of Electrical and Electronics Engineering, ³Dept. of Fundamental and Applied Sciences,
Universiti Teknologi Petronas, Perak, Malaysia

⁴Dept. of Physics, COMSATS Institute of Information Technology, Islamabad, Pakistan

mtaha.jilani@gmail.com, wong_pengwen@petronas.com.my

Abstract. This article describes the modeling of biological tissues at microwave frequency using equivalent lumped elements. A biosensor based on microstrip ring resonator (MRR), that has been utilized previously for meat quality evaluation is used for this purpose. For the first time, the ring-resonator loaded with the lossy and high permittivity dielectric material, such as biological tissue, in a partial overlay configuration is analyzed. The equivalent circuit modeling of the structure is then performed to identify the effect of overlay thickness on the resonance frequency. Finally, the relationship of an overlay thickness with the corresponding RC values of the tissue equivalent circuit is established. Simulated, calculated and measured results are then compared for validation. Results agreed well while the observed discrepancy is in an acceptable limit.

Keywords

Microwave biosensor, microstrip ring resonator, equivalent circuit modeling, effective permittivity, dielectric constant, meat dielectric characterization, overlay thickness.

1. Introduction

Over a decade, electrical properties of materials have gained significant research interest. The measurement of these properties is considered as most promising research area in the field of medical, agriculture and materials engineering [1]. The main advantage of these methods is the non-invasive and non-destructive evaluation, which is desirable for many in-line industrial applications. It is due to the fact that the interaction of electromagnetic fields with a material can be investigated to understand the underlying physical properties of the material. Whereas, this interaction is mainly governed by the relative permittivity, loss factor and conductivity of a material [2]. When a dielectric material is subjected to the electromagnetic field, its behavior can be defined by [3]

$$\varepsilon^* = \varepsilon' - j \varepsilon'' \quad (1)$$

where $j = \sqrt{-1}$, ε' is the real part called dielectric constant and the imaginary part is a loss factor. The dielectric constant describes the ability of a material to store energy, whereas, the loss-factor defines energy dissipation of a material. Another, important property of a material to conduct an electric current is known as conductivity σ and it is given as [2]

$$\tan \delta = \sigma / \omega \varepsilon_0 \varepsilon_r \quad (2)$$

where $\tan \delta$ is tangent-loss which is the ratio between loss factor and dielectric constant, ω is the angular frequency, ε_0 is the free space permittivity and ε_r is the dielectric constant of the material. These properties can be utilized effectively, once their relationship can be established with the physical attributes of a material.

In food industry, the application of dielectric properties is evident into various products, such as agriculture, edible-oil, dairy, and meat. Particularly in meat industry, due to increasing demand for high quality products and strict regulations for health and safety. The need for an effective, online and non-destructive dielectric technique is become obvious. Several efforts have been attempted to identify the relationship of dielectric properties with the quality attributes, like: moisture content, composition, freshness, aging, discrimination of frozen & thawed products and microbial activities [4]. Similarly, various new techniques have been proposed and adopted to determine the complex permittivity. Since, biological tissues are heterogeneous, anisotropic and semi-solid in nature, practically only few techniques are preferred for the measurements. The most widely used technique is the coaxial probe, which exhibits high accuracy for broadband measurements [2]. It is based on reflection principle, and it is successfully utilized for determination of meat-aging [5], frozen detection [6], fat analysis [7], and to study the temperature effect [8]. Although, this method has higher accuracy but still is subject to errors. The main source of errors are sample thickness (at least semi-infinite for probe) and the air-gap between the sample and a probe, it is reported that they can introduce errors of up to 20% [9]. The irregularities on a sample surface can reduce accuracy, therefore to decrease error rate MUT should be smoothen. However,

sample preparation will become a challenging task for this method. Cable stability during measurements should be considered, since the phase changes cause some additional errors [3]. Repetitive calibration of a measurement system is required to reduce errors.

Recently, a relatively newer method based on microstrip ring-resonator has been used for meat quality evaluation [10], [11]. Obtained results are satisfactory while compared to existing approaches [12]. Since, ring resonator is based on resonance; it offers higher accuracy than other simple planar structures. Additionally, it is simple, cost-effective, fast (measurements in few seconds) and provides higher Q-factor (~250) than conventional microstrip line [13]. Sample loading and unloading is relatively easier than other comparable resonance techniques. This method is based on a fact that the effective permittivity of a planar resonator is strongly dependent on the permittivity of the region or overlay above the ring surface [1]. Hence, any permittivity variations due to physical properties of the material can be evaluated.

In this study equivalent circuit modeling of a biological tissue loaded resonator is performed. The structure of this article is as follows: initially the equivalent lumped elements of the ring structure are derived using transmission line analysis. A thorough study is then carried out to consider the losses, radiation and coupling effects associated to the ring-resonator structure. Similarly, the equivalent circuit of the biological tissue is discussed. The effect of tissue thickness on the resonance frequency and corresponding RC values are studied. This has been used to identify the relationship between RC components & permittivity and then established with overlay thickness. Finally, the resonance frequency of the sample loaded ring-resonator is computed and validated with the measured results.

2. Theoretical Analysis and Modeling of Microwave Biosensor

The microstrip ring resonator is considered as a closed-loop transmission line. To excite the resonator, power is capacitively coupled through feed lines and the gap between them, as shown in Fig. 1(a). The resonance is produced when a mean circumference of the ring is equal to an integral multiple of the guided wavelength [14]

$$2 \pi r = n \lambda_g \quad \text{for } n = 1, 2, 3 \dots \quad (3)$$

where r is the ring radius, n is mode number and λ_g is the guided wavelength. For resonance frequency, considering (3) with λ_g will give

$$f_0 = \frac{nc}{2\pi r \sqrt{\epsilon_{eff0}}} \quad (4)$$

where f_0 is the resonance frequency, c is the speed of light in free-space and ϵ_{eff0} is the effective permittivity of the ring resonator. Once the unloaded resonance frequency is de-

termined, the effective permittivity with the sample loaded ring-resonator can be evaluated by [13]

$$\epsilon_{eff1} = \epsilon_{eff0} \left(\frac{f_0}{f_1} \right)^2 \quad (5)$$

where ϵ_{eff1} and f_1 are the sample-loaded effective permittivity and resonance frequency, respectively.

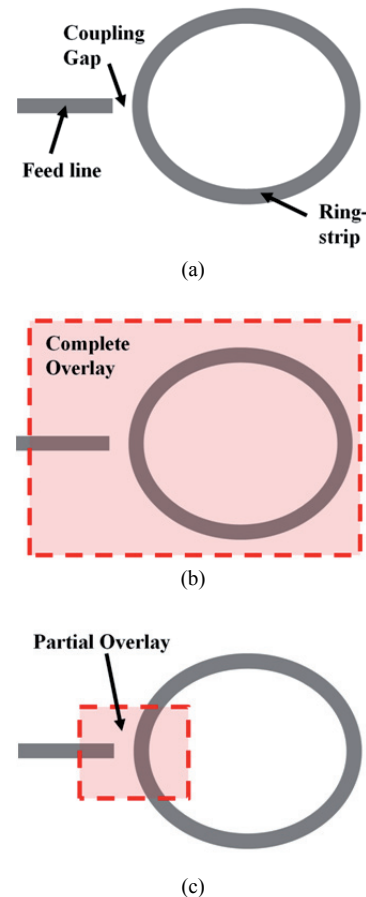


Fig. 1. Microwave biosensor based on one-port microstrip ring-resonator: (a) without a sample, (b) with complete overlay sample, (c) with partial overlay sample.

The structure of microstrip has been widely analyzed, several numerical and dispersion models are used to determine the resonant frequency and effective permittivity. Broadly speaking, these methods of analysis can be classified into two categories; quasi-static analysis and full-wave analysis [15]. In quasi-static approach the propagation mode assumed to be pure TEM and analysis is performed by considering electrostatic capacitance of the structure. In the contrary, for full-wave analysis the propagation mode is hybrid in nature, thus, it is more accurate. Although, the variation of effective permittivity and characteristics impedance can also be studied with respect to the frequency, but altogether make it analytically complex.

Considering quasi-static solutions, the most common techniques are conformal mapping approach (CMA) and the variational method [15]. Although, the results from these two methods are good enough, however, they are

limited to only complete dielectric overlay structures, as depicted in Fig. 1(b). In recent study, it is found that due to strong electric fields in the coupling gap, this region has maximum sensitivity to the above surface permittivity variations [16]. Here, field perturbations in this region are linearly proportional to the resonance shifts [17], even this tendency remains same for further higher order modes. Utilizing the partial overlay arrangement, as shown in Fig. 1(c), a small size sample can also be evaluated, while the complete overlay requires relatively a larger sample size. This type of overlay, in fact provides flexibility for the measurement of most of the biomaterials, including grain and pulverized samples [18]. It has been reported that, the said configuration provides an appreciable shift in resonance for the materials having moisture content greater than 15 % [16]. Likewise, for the biological tissues having moisture in 72-80 % range, overlaid on coupling region can produce higher resonance shifts. Although, this arrangement seems more suitable for permittivity measurements, yet, no attempt has been made to analyze the partial overlay arrangement.

Only few reports have discussed the partial overlay configuration, however, they just limited to some specific cases [18], [19]. An empirical expression is obtained, using a ring resonator designed at 10 GHz using Al_2O_3 substrate [18]. Here, the material is partially overlaid on ring-structure to extract the dielectric constant using curve-fitted expression. However, this expression has limited size range and is only applicable to the given resonator.

An alternative solution to numerical and curve-fitted models is an equivalent circuit modeling that can provide a simple and quick analysis, without any time consuming computation [20]. Although, numerical methods give accurate and rigorous results, however, with increased complexity they are difficult to use [14]. Analyzing with these methods often requires large computing time and space for storage. While, circuit analysis can be easily modeled while considering the structure variations and discontinuities [14]. In the following section, we will discuss the modeling scheme to encompass the RLC model of a capacitively-coupled ring-resonator and a tissue structure.

2.1 Equivalent Circuit for a Microstrip Ring Resonator and Biological Tissues

The most straightforward method to analyze the microstrip ring resonator is an equivalent lumped element circuit. It can be described as a simple parallel RLC circuit using the transmission line theory [21], as depicted in Fig. 2(b). This equivalent circuit has parallel connected RLC components, which are associated with the ring losses in terms of resistance R_r and the resonance frequency that corresponded to the particular inductance L_r and capacitance C_r . The series capacitance C_g represents the coupling strength while the additional parallel resistance R_f caters the losses incurred due to feed line. The resonance of the circuit, assuming negligible gap-capacitance, can be calculated as

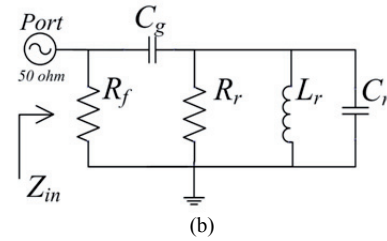
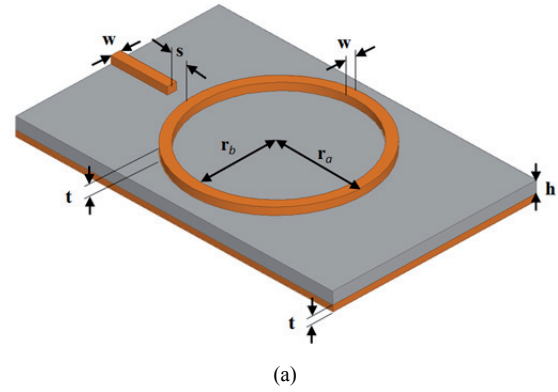


Fig. 2. Capacitively coupled ring resonator: (a) layout, (b) equivalent RLC circuit.

$$f_0 = \frac{1}{2\pi \sqrt{L_r C_r}} \quad (6)$$

However, to derive the input impedance of the ring same approach has been used as described in [21]. Assuming that the port 2 of a ring-resonator is an open circuit ($i_2 = 0$), where equally divided two-line sections, l_1 and l_2 forms a parallel circuit. Therefore, for a circuit with the individual lengths of transmission lines, the ABCD matrix is given by

$$\begin{bmatrix} A & B \\ C & D \end{bmatrix}_{1,2} = \begin{bmatrix} \cosh(\gamma l_{1,2}) & Z_0 \sinh(\gamma l_{1,2}) \\ Y_0 \sinh(\gamma l_{1,2}) & \cosh(\gamma l_{1,2}) \end{bmatrix}, \gamma = \alpha + j\beta \quad (7)$$

where subscripts 1 and 2 correspond to the transmission lines l_1 and l_2 respectively, Z_0 is the characteristics impedance which is equal to $1/Y_0$, γ is the propagation constant, α is the attenuation constant and β is the phase constant. Similarly, the converted ABCD-matrix into Y-matrix is given as [21]

$$\begin{bmatrix} Y_{11} & Y_{21} \\ Y_{12} & Y_{22} \end{bmatrix} = \begin{bmatrix} Y_0[\coth(\gamma l_1) + \coth(\gamma l_2)] & -Y_0[\operatorname{csch}(\gamma l_1) + \operatorname{csch}(\gamma l_2)] \\ -Y_0[\operatorname{csch}(\gamma l_1) + \operatorname{csch}(\gamma l_2)] & Y_0[\coth(\gamma l_1) + \coth(\gamma l_2)] \end{bmatrix} \quad (8)$$

Letting $i_2 = 0$, the input impedance of the ring (Z_{ring}) can be found by

$$Z_{ring} = \frac{V_1}{i_1} \Big|_{i_2=0} = \frac{Z_0}{2} \frac{\sinh(\gamma l)}{\cosh(\gamma l) - 1} \quad (9)$$

Let $l_g = l/2 = \lambda_g/2$, the Z_{ring} can be re-written as

$$Z_{ring} = \frac{Z_0}{2} \frac{1 + j \tanh(\alpha l_g) \tan(\beta l_g)}{\tanh(\alpha l_g) + j \tan(\beta l_g)} \quad (10)$$

Generally, transmission lines have small loss, so the attenuation can be assumed as $\alpha l_g \ll 1$ and then $\tanh(\alpha l_g)$

$\approx \alpha l_g$. Considering $\beta = v_p/\omega$, where v_p is the phase velocity and ω is the angular velocity, with some further manipulations [21], Z_{in} can be approximated as

$$Z_{ring} \cong \frac{Z_0}{2} \frac{1 + j\alpha l_g \pi \Delta \varpi / \varpi_0}{\alpha l_g + \pi \Delta \varpi / \varpi_0}. \quad (11)$$

Recalling that $\alpha l_g \ll 1$, similarly $\alpha l_g \pi \Delta \omega / \omega_0 \ll 1$ thus

$$Z_{ring} \cong \frac{Z_0 / 2\alpha l_g}{1 + j\pi \Delta \varpi / \alpha l_g \varpi_0}. \quad (12)$$

In general, the input impedance given for a parallel GLC resonant circuit is

$$Z_i = \frac{1}{G + 2j\Delta \varpi C}. \quad (13)$$

Comparing equation (12) with (13), the obtained expression of Z_{ring} is similar to the parallel GLC circuit. Subsequently, the resistance R_r of the ring will be

$$G_r = \frac{1}{R_r} = \frac{2\alpha l_g}{Z_0} = \frac{\alpha \lambda_g}{Z_0} \quad (14)$$

while the inductance L_r can be derived from $\omega_0 = 1/\sqrt{L_r C_r}$ and is given as

$$L_r = 1/\varpi_0^2 C_r, \quad (15)$$

and finally, the capacitance of the ring circuit is

$$C_r = \frac{\pi}{Z_0 \varpi_0}. \quad (16)$$

Although, the ring's equivalent RLC component equations has been derived, however, it should be noted that this circuit analysis does not include the losses pertaining to radiation effects. Henceforth, the total losses R_r along with radiation loss can be described as:

$$R_r = \frac{1}{\left(\frac{1}{R_{rad}} + \frac{1}{R_{cond}} + \frac{1}{R_{dielec}} \right)} \quad (17)$$

where R_{rad} are the losses incurred due to radiation, R_{cond} are the losses due to finite conductivity of copper and R_{dielec} are the dielectric losses. The dielectric loss is given as

$$R_d = \frac{Z_0}{\alpha_d l_g} \text{ Np/m} \quad (18)$$

where the attenuation constant for a dielectric loss α_d is described as [22]

$$\alpha_d = 27.3 \frac{\epsilon_r}{\epsilon_r - 1} \frac{\epsilon_{eff} - 1}{\sqrt{\epsilon_{eff}}} \frac{\tan \delta}{\lambda_0}. \quad (19)$$

Similarly, for the conductor, the loss is

$$R_c = \frac{Z_0}{\alpha_c l_g} \text{ Np/m} \quad (20)$$

where the attenuation constant for the ohmic loss α_c is defined as

$$\alpha_c = \frac{8.68 R_{s1}}{2\pi Z_0 h} \left[\frac{w_{eff}}{h} + \frac{w_{eff}}{\pi h} \frac{w_{eff}}{2h} + 0.94 \right] \cdot \left[1 + \frac{h}{w_{eff}} + \frac{hV}{\pi w_{eff}} \right]. \quad (21)$$

$$\left[\frac{w_{eff}}{h} + \frac{2}{\pi} \ln \left\{ 2\pi e \left(\frac{w_{eff}}{2h} + 0.94 \right) \right\} \right]^{-2}$$

while,

$$\begin{aligned} V &= \ln \left(\frac{2h}{t} \right) + \frac{t}{w}, \\ R_{s1} &= R_s \cdot \left[1 + \frac{2}{\pi} \tan^{-1} \left\{ 1.4 \left(\frac{\Delta}{\delta_s} \right)^2 \right\} \right], \\ R_s &= \sqrt{\frac{\pi f \mu_0}{\sigma}} \end{aligned} \quad (22)$$

where R_{s1} is the surface-roughness resistance of the conductor, e is the naperian base, R_s is the conductor's surface resistance, Δ is the surface roughness, $\delta_s = 1/\sqrt{R_s \sigma}$ is the skin depth, σ is the conductivity, f is the frequency, μ_0 is the free-space permeability, t and w are the line thickness and width, respectively.

As it is mentioned before, transmission line analysis does not account for the radiation loss, whereas, full wave analytical solutions can provide the better insight to this loss mechanism. However, using the cavity resonator model few simple assumptions have been made to reduce unnecessary complexity, as outlined in [23], thus the radiation can be given as

$$R_{rad} = \frac{V_0^2}{2P_r} \quad (23)$$

where V_0 is the voltage produced at the edge of the ring and P_r is the radiated power from the ring. Therefore:

$$V_0 = E_0 h \left[J_n(k_n b_e) Y_n'(k_n a_e) - J_n'(k_n a_e) Y_n(k_n b_e) \right], \quad (24)$$

$$P_r = \frac{2h^2 E_0^2}{\pi \eta_0 \epsilon_r} I_1, \quad (25)$$

$$I_1 = \int_0^{\frac{\pi}{2}} \left[\frac{n^2 \cos^2 \theta}{k_0^2 \sin \theta} \left(\frac{J_n(k_0 a_e \sin \theta)}{a_e} - \frac{J_n'(k_n a_e)}{J_n'(k_n b_e)} \frac{J_n(k_0 b_e \sin \theta)}{b_e} \right)^2 + \sin \theta \left(J_n'(k_0 a_e \sin \theta) - \frac{J_n'(k_n a_e)}{J_n'(k_n b_e)} J_n'(k_0 b_e \sin \theta) \right)^2 \right] d\theta \quad (26)$$

Finally, using (23) the radiation loss can be easily determined. However, in case of an overlay dielectric layer, this loss will be reduced substantially [24].

For a gap-coupled ring-resonator, power coupled to the resonator through feed lines and coupling gaps [14].

Here, with a small gap the coupling will be tight and the gap-capacitance becomes appreciable. This coupling region has maximum electric fields and as reported previously, it will be more sensitive to overlay permittivity variations [16]. Although, this increase in gap-capacitance causes more sensitivity, however, it even deviates the resonator's inherent frequency to the lower frequency, which is known as "pushing effect" [25]. This pushing effect though lowers the insertion-loss but its effect on resonance frequency is more significant [14]. Hence, it cannot be neglected (as in the case of loose coupling) and for more accurate analysis it has to be considered. The gap capacitance can be modeled as π -network, as reported in [26]. The fringing fields are modeled as shunt capacitances C_f which are due to the edges of the strip, while the series capacitance C_g is assumed to be the result of coupling mechanism:

$$C_f = \frac{C_{even}}{2}, \quad (27)$$

$$C_g = \frac{\left(C_{odd} - \frac{C_{even}}{2}\right)}{2}. \quad (28)$$

Closed form-expressions for C_{odd} and C_{even} are described in [27], with their corrected form [24] and they are re-modified as:

$$\frac{C_{odd}}{w} = \left(\frac{s}{w}\right)^{m_0} e^{k_0} \quad \text{pF/m} \quad (29)$$

$$\frac{C_{even}}{w} = 12 \left(\frac{s}{w}\right)^{m_e} e^{k_e}$$

where, for our considered s/w ratio

$$m_0 = \frac{w}{h} (0.619 \log w/h - 0.3853) \quad (\text{for } 0.1 \leq s/w \leq 1.0)$$

$$K_0 = 4.26 - 1.453 \log w/h \quad (30)$$

$$m_e = 0.8675 \quad (\text{for } 0.1 \leq s/w \leq 0.3)$$

$$K_e = 2.043(w/h)^{0.12}$$

The modified expressions for low ϵ_r substrate are given as

$$C_{even}(\epsilon_r) = 1.167 \cdot C_{even}(9.6) \cdot \left(\frac{\epsilon_r}{9.6}\right)^{0.9}, \quad (31)$$

$$C_{odd}(\epsilon_r) = 1.1 \cdot C_{odd}(9.6) \cdot \left(\frac{\epsilon_r}{9.6}\right)^{0.8}. \quad (32)$$

Now considering the effect of the gap-capacitance, the resonance frequency given in (6), can be modified as

$$f_0 = \frac{1}{2\pi \sqrt{L_r (C_r + C_g)}}. \quad (33)$$

Finally, a one-port microstrip ring resonator is designed at 1 GHz frequency for measurement purpose.

A low loss substrate Roger RT/Duriod 5880 with the dielectric constant ϵ_r of 2.2 and the loss $\tan\delta$ of $9 \cdot 10^{-4}$ is used. Strip width and effective permittivity are determined by using LineCalc of Agilent ADS. The corresponding width for 50 Ω characteristics impedance is calculated as 2.4 mm while the ϵ_{eff} was 1.875. The tight coupling mechanism is incorporated using 250 μm gap size. A feed line with a typical length of a 35 mm is used. The structure is designed and then simulated in FEM based 3D solver HFSS.

Furthermore, using the derived expressions for the equivalent R, L, and C of ring and gap-capacitance, the corresponding values are computed. Since, for the feed loss R_f the exact value is not well defined, due to complex field distribution near the coupling region. Hence, a computer program is used to fit its value to simulation data. The circuit simulation is then performed by using Agilent ADS. Finally, for a fabrication of microstrip ring-resonator a standard photolithography procedure is adapted to print the ring structure on substrate. Design parameters are tabulated in Tab. 1

Parameter	Designed Value
Substrate	Roger RT/Duriod 5880 ϵ_r 2.2, $\tan\delta$ $9 \cdot 10^{-4}$
Substrate height	787 μm
Copper thickness	17.5 μm
Coupling gap	250 μm
Line Width (Feed & Ring)	2.4 mm
Feed line length	35 mm
Frequency	1 GHz

Tab. 1. Design parameters of the proposed MRR.

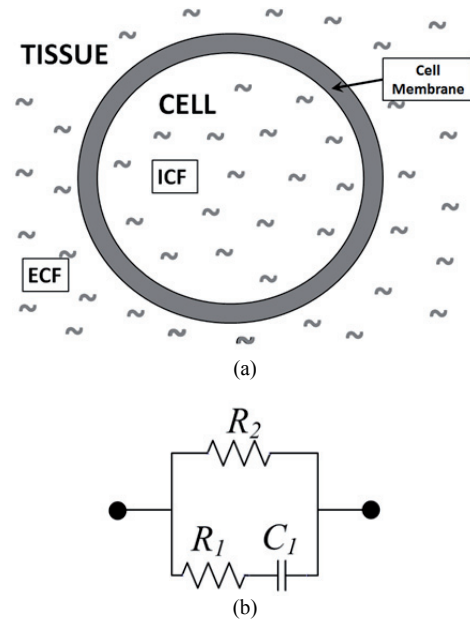


Fig. 3. Biological tissue: (a) structure— ECF is an extracellular fluid and ICF is an intracellular fluid; (b) equivalent circuit.

The structure of biological tissue and its equivalent circuit are shown in Fig. 3. As depicted in Fig. 3(a), the tissue contains extracellular fluid (ECF), this fluid behaves as an electrolyte which mainly comprises Na^+ and Cl^- ions [28]. Cells are immersed into ECF and each cell is basically surrounded by a leaky dielectric membrane that encloses the conductive fluid which is commonly known as intra-cellular fluid (ICF) [29]. This inner plasma suspension is basically called *cytoplasm* and it mainly consists on K^+ ions.

The equivalent circuit of tissues is widely discussed in literature, the typical RC combination, as shown in Fig. 3(b), is presented in many articles [28], [30]. The modeling of a cell structure is complex and extremely difficult, however, various effects related to the fields interaction can be defined by using a simple cell model [31]. At higher frequencies the electric field interacts mainly at cellular level and its behavior can be represented by RC circuit, as shown in Fig. 3(b). The series resistance R_1 basically describes the resistive property of the intracellular fluid. Whereas, the series capacitance C_1 actually represents the capacitive behavior of a cellular-membrane, the parallel resistance R_{12} exhibits the resistive nature of an extracellular fluid. As we have discussed before, at low frequencies, in lower kHz range, the current flows mainly through the extracellular fluid, depicted in Fig. 4(a). This is due to the fact that the cellular membrane is highly resistant to the applied electric field of lower frequency, where the current flow through only ECF. At this point, the impedance is very high, however, as the frequency increases impedance decreases as resistance drops due to its predominant capacitive behavior [32]. In the contrary, at higher frequencies the current starts penetrating into cells, typically from MHz

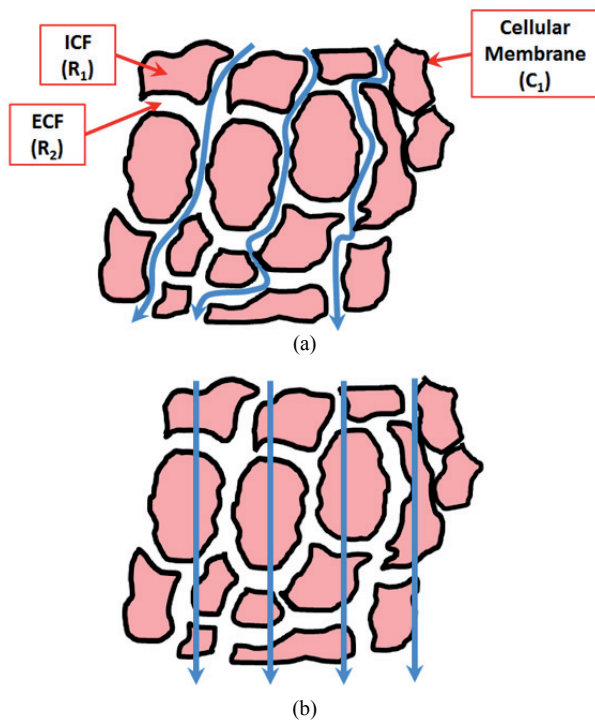


Fig. 4. The flow of electric current through tissue: (a) at low frequencies; (b) at higher frequencies.

region. This can be observed from Fig. 4(b), where at higher frequencies (MHz range and above) the outer membrane now becomes transparent [31]. Since the membrane is shortened at higher frequencies the impedance becomes zero, hence, the field lines are passed more uniformly at higher frequencies [32].

2.2 Modeling of RLC Components of the Capacitively Coupled Dielectric Loaded Ring-Resonator

The expressions for input-impedance, gap-capacitance and lumped elements of a ring-resonator are already derived. Their values corresponding to the parameters that are tabulated in Tab. 1 are then used in Agilent ADS to model the equivalent circuit. Similarly, for the resonator loaded with a meat sample, the equivalent circuit of a tissue (i.e. Fig. 3(b)) will be connected in parallel to the C_g of a ring resonator (i.e. Fig. 2(b)). Using meat equivalent circuit tuning in ADS, the values of R_1 , C_1 and R_2 are extracted. These values are based on the data obtained by full-wave simulation on HFSS, for the samples with different thicknesses. To validate the simulation results, the basic circuit theory of a transmission line is used. For this purpose, initially an unloaded capacitively coupled microstrip ring resonator is analyzed. The transfer matrix of a gap capacitance C_g is obtained

$$[T]_{C_g} = \begin{bmatrix} 1 & -j \\ 0 & 1 \end{bmatrix}. \quad (34)$$

The impedance of a ring Z_{ring} is already calculated using (10). Now, considering ABCD parameters of (34) and Z_{ring} as a load impedance, the total input impedance of a capacitively coupled microstrip ring resonator can be evaluated from:

$$Z_{in} = \frac{AZ_L + B}{CZ_L + D}. \quad (35)$$

Hence, the return loss can be obtained by

$$S_{11} = \frac{Z_{in} - Z_0}{Z_{in} + Z_0}. \quad (36)$$

In a similar manner, the meat loaded ring resonator is analyzed, where the equivalent circuit of a meat sample is connected in parallel to the ring resonator. The analysis begins with a transfer (ABCD) matrix of a meat equivalent circuit. Thus, for a series resistance R_2 [T] is given as:

$$[T]_{R_2} = \begin{bmatrix} 1 & R_2 \\ 0 & 1 \end{bmatrix}. \quad (37)$$

Similarly, for a series resistance R_1 and capacitances C_1 the product of the obtained transfer matrices will be

$$[T]_{R_1 * C_1} = \begin{bmatrix} 1 & -j \\ 0 & 1 \end{bmatrix} + R_1. \quad (38)$$

Considering the shunt elements, (37) and (38) are converted into Y-parameters respectively, which yields

$$\begin{aligned}
 [Y]_{R1} &= \begin{bmatrix} \frac{1}{R_2} & -\frac{1}{R_2} \\ \frac{1}{R_2} & \frac{1}{R_2} \end{bmatrix} \\
 [Y]_{C1} &= \begin{bmatrix} \frac{1}{\omega C_1} & -\frac{1}{\omega C_1} \\ -\frac{j}{\omega C_1} + R_1 & \frac{-j}{\omega C_1} + R_1 \end{bmatrix} \quad (39)
 \end{aligned}$$

Further, for the gap capacitance $[T]_{Cg}$ is converted into Y-matrix, thus

$$[Y]_{Cg} = \begin{bmatrix} \frac{1}{\omega C_g} & -\frac{1}{\omega C_g} \\ -\frac{j}{\omega C_g} & \frac{-j}{\omega C_g} \end{bmatrix} \quad (40)$$

Adding, $[Y]_{R1} + [Y]_{C1} + [Y]_{Cg}$ will give the overall Y-parameters that will transform back into ABCD parameters using

$$\begin{bmatrix} A & B \\ C & D \end{bmatrix} = \begin{bmatrix} \frac{-Y_{22}}{Y_{21}} & -\frac{1}{Y_{21}} \\ \frac{Y_{12} \cdot Y_{21} - Y_{11} \cdot Y_{22}}{Y_{21}} & \frac{-Y_{11}}{Y_{21}} \end{bmatrix} \quad (41)$$

Thus, again using (35) and (10) Z_{in} can be extracted for the meat sample loaded resonator.

3. Results and Discussion

The equivalent circuit modeling of unloaded and loaded microstrip ring resonator is performed. In Fig. 5, the measured, simulated and calculated results are presented. Obtained results are in good agreement; it can be seen that the resonance is produced over the regular 1 GHz intervals in the given range. However, due to the tight coupling mechanism, the “pushing effect” causes the deviation of a resonator’s inherent frequency to a lower frequency. In this case the reflection loss observed from the calculation was 0.981 GHz while from the simulation results it is observed at 0.980 GHz and from measurement it was 0.978 GHz. In measured results the noise figure is higher, that might be the result of limited calibration of portable equipment. But still, the overall difference between these results is not more than 0.3 %.

Further, the simulation result is analyzed for the sample loaded ring resonator over the range from 5 μm to 16 mm. This range is chosen, while considering the results

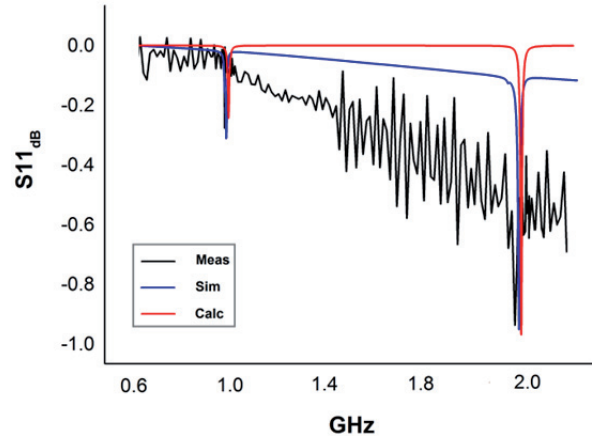


Fig. 5. Reflection loss – Measured, Simulated and Calculated of unloaded microstrip ring resonator.

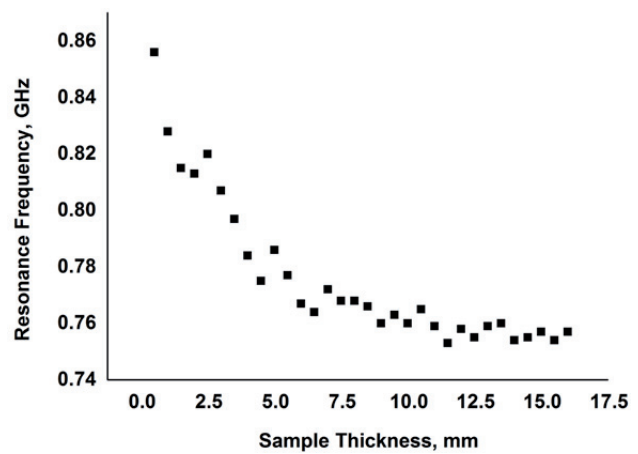


Fig. 6. Resonance frequency as a function of overlay thickness.

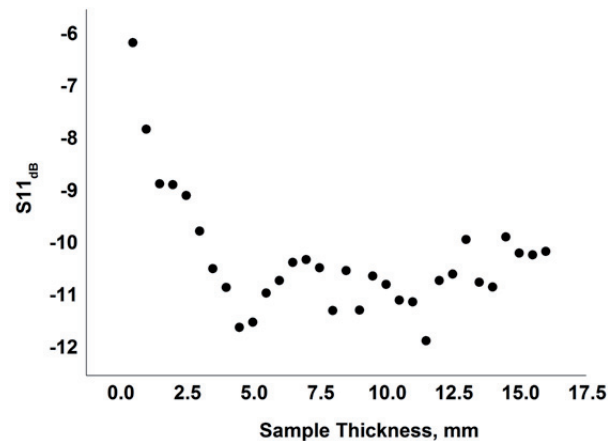


Fig. 7. Return loss as a function of overlay thickness.

of previous study [33], where beyond a certain point, the size of a meat sample will not affect the effective permittivity significantly. Since the thickness effect is more significant than the effect of width, in this study, the width is fixed to 18.3 % of λ_g . Here, beyond this width the effect on resonance frequency is negligible. In Fig. 6 and 7, the resonance frequency and return loss are presented as a function of overlay thickness, respectively. Considering Fig. 6, it can be seen that as the sample thickness increases, the

resonance frequency decreases. This is due to the fact that as the sample size increases the field perturbation is also increased, since more fringing fields are getting concentrated into the sample. That results into increasing fringing field capacitance, hence decreases the resonance frequency. Although the shift in resonance frequency is significant but it limited to a lower range only, where beyond a certain thickness, its effect is not significant. Similarly, this happens to the magnitude of the return loss also (Fig. 7), where beyond that point the thickness will not affect the loss effectively. This behavior can be interpreted as the effective permittivity also increases with the overlay height until it reaches the asymptotic value, which indicates that all of the electric field is confined into overlay and substrate [34].

In Fig. 8 and 9, for the given sample thickness the resistive behavior of intracellular fluid and capacitive behavior of cell membrane is presented, respectively. When an electric field is applied to a tissue, the current will pass through the ECF or in some cases, through both ECF and ICF [30]. The path containing ECF is a purely resistive; while for ICF other than resistive it also includes the capacitive effect of a membrane, thus makes it frequency dependent. It is worth to mention that the resistance R_1 and capacitance C_1 of the cell structure are linearly related to

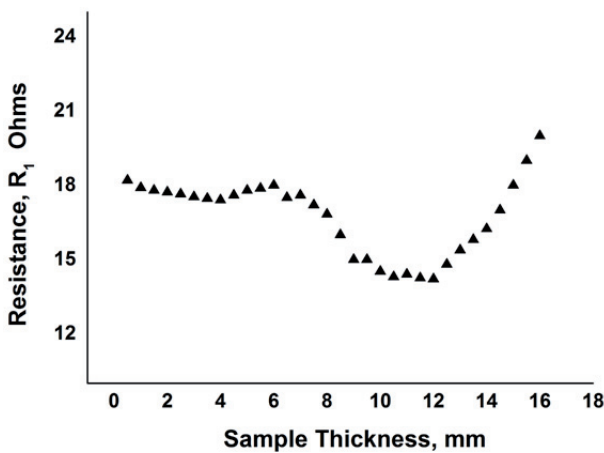


Fig. 8. Resistance of an intracellular fluid as a function of overlay thickness.

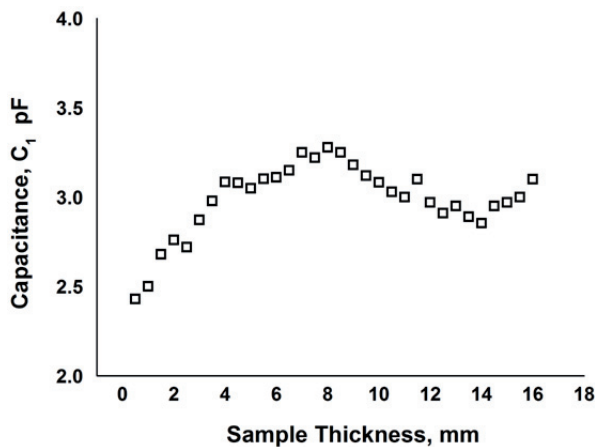


Fig. 9. Capacitance of cell membrane as a function of overlay thickness.

the resistivity of ICF and the dielectric constant of a membrane, respectively [31]. Thus, the effect of resistance is obvious on the magnitude of the resonance and similarly, the capacitance effect is apparent on the resonance shift. The resistance R_1 slightly decreases initially, but the transition is observed at thickness threshold, after that it increases rapidly. This rapid change in R_1 values is more than 27 %, which can be described as the lossy nature of intracellular fluid that contains K^+ ions. The thickness mainly contributes to the increase in resistive losses of the inner suspension.

As it can be seen in Fig. 9, the membrane capacitance C_1 increases up to thickness threshold, after that it seems somehow constant. This behavior of membrane capacitance seems to be inversely proportional to the resonance frequency shift, as f_1 decreases C_1 increases. Initially, the value of C_1 changes about 34.8 % up to the transition range. Beyond that range, there is minimum variation in their values, which is about 6 % only.

In Fig. 10, the resistance R_2 is given as a function of the sample thickness. This resistance exhibits the behavior of extracellular fluid (ECF), where it decreases till the thickness saturation range, but beyond that point the resistance value has minimum variation. The effect on R_2 is significant where it drops approximately from 335 Ω to 200 Ω (gives 40.3 % change) but beyond that transition point the change in its values is not more than 15 %.

Finally, the measurements are carried out using the same procedure as reported in [33]. The measured resonance shift, corresponding to different thicknesses is then

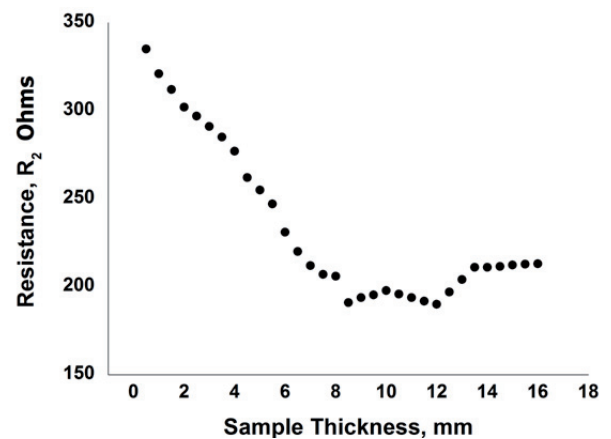


Fig. 10. Resistance of an extracellular fluid as a function of overlay thickness.

Results	Resonance Shift (MHz)	
	10 mm	15 mm
Simulated	213	218
Calculated	153	151
Measured	198	202

Tab. 2. Acquired resonance shift - from simulated, calculated and measured results for the 10 mm and 15 mm thick overlay biological tissues.

compared for validation of computed results. In Tab. 2 the comparison of simulated, calculated and measured results is presented. The observed discrepancy is within the acceptable limit, where the maximum difference observed between the measured and simulated values is about 7.5 %. It is due to actual physical properties of the samples used for measurements, handling and cutting of meat samples can change the amount of moisture, thus having significant effect on resonance frequency. Further, it is really hard to get the exact dimension of meat samples for measurements, due to its malleable nature. This can be also a possible reason for this discrepancy. The values obtained by simulation data are higher than those that are calculated; with a difference of about 24 %. The main reason of this difference is the FEM based full-wave analysis that utilizes the hybrid propagation mode, which involves complex analysis to make it more accurate. Additionally, in full-wave simulation variation of effective permittivity and characteristics impedance with respect to frequency is also performed. Although, transmission line theory can provide sufficient analysis but still it has its own limitations.

4. Conclusion

In this study a thorough analysis of a microwave biosensor based on a dielectric loaded microstrip ring resonator is performed. For the first time, a partial overlay arrangement of a lossy and high permittivity dielectric material, like biological tissue, on ring resonator is analyzed. The values of the lumped components of a 1GHz unloaded resonator are first determined and then, their response is compared with the simulated and measured results. The results are well agreed and the overall difference is not more than 0.3 %. For the loaded sensor, the relationship of overlay thickness with the RC values of the tissue model is established using equivalent circuit modeling. Finally, the resonance frequency of the sample loaded ring resonator is computed and validated with the measured results. The results are in good agreement while the observed discrepancy is in the acceptable limit.

References

- [1] VENKATESH, M. S., RAGHAVAN, G. S. V. An overview of dielectric properties measuring techniques. *The Journal of the Canadian Society for Bioengineering (CSBE)*, 2005, vol. 47, p. 7.15–7.30.
- [2] ZAJÍČEK, R., OPPL, L., VRBA, J. Broadband measurement of complex permittivity using reflection method and coaxial probes. *Radioengineering*, 2008, vol. 17, no. 1, p. 14–19.
- [3] AGILENT-TECHNOLOGIES, *Basics of Measuring the Dielectric Properties of Material*. CA, USA, 2006.
- [4] DAMEZ, J.-L., CLERJON, S. Meat quality assessment using biophysical methods related to meat structure. *Meat Science*, 2008, vol. 80, no. 9, p. 132–149.
- [5] DAMEZ, J.-L., CLERJON, S., ABOUELKARAM, S., LEPETIT, J. Beef meat electrical impedance spectroscopy and anisotropy sensing for non-invasive early assessment of meat ageing. *Journal of Food Engineering*, 2008, vol. 85, p. 116–122.
- [6] BASARAN-AKGUL, N., BASARAN, P., RASCO, B. A. Effect of temperature (-5 to 130 degrees C) and fiber direction on the dielectric properties of beef Semitendinosus at radio frequency and microwave frequencies. *Journal of Food Science*, Aug 2008, vol. 73, no. 6, p. E243-9.
- [7] SING, K. NG., GIBSON, A., PARKINSON, G., HAIGH, A., AINSWORTH, P., PLUNKETT, A. Bimodal method of determining fat and salt content in beef products by microwave techniques. *IEEE Transactions on Instrumentation and Measurement*, 2009, vol. 58, no. 10, p. 3778–3787.
- [8] TRABELSI, S. N., STUART O. Use of dielectric spectroscopy for determining quality attributes of poultry meat. In *Annual International Meeting of the American Society of Agricultural and Biological Engineers (ASABE)*. June 21-24, 2009, no. 097035, p. 8.
- [9] HAGL, D. M., POPOVIC, D., HAGNESS, S. C., BOOSKE, J. H., OKONIEWSKI, M. Sensing volume of open-ended coaxial probes for dielectric characterization of breast tissue at microwave frequencies. *IEEE Transactions on Microwave Theory and Techniques*, 2003, vol. 51, p. 1194–1206.
- [10] JILANI, M. T., WEN, W. P., ZAKARIYA, M. A., CHEONG, L. Y. Dielectric method for determination of fat content at 1 GHz frequency. In *5th International Conference on Intelligent and Advanced Systems*. Kuala Lumpur (Malaysia), June 2014.
- [11] JILANI, M. T., WEN, W. P., ZAKARIYA, M. A., CHEONG, L. Y. Microstrip ring resonator based sensing technique for meat quality. In *IEEE Symposium on Wireless Technology and Applications*. Kuching (Malaysia), 2013.
- [12] JILANI, M. T., WEN, W. P., ZAKARIYA, M. A., CHEONG, L. Y. A microwave sensor for non-destructive dielectric characterization of biological systems. *Journal of Microwaves, Optoelectronics and Electromagnetic Applications*, 2014 (accepted for publication).
- [13] BERNARD, P. A., GAUTRAY, J. M. Measurement of dielectric constant using a microstrip ring resonator. *IEEE Transactions on Microwave Theory and Techniques*, 1991, vol. 39, no. 3, p. 592 to 595.
- [14] CHANG, K., HSIEH, L. H. *Microwave Ring Circuits and Related Structures*. John Wiley & Sons, 2004.
- [15] GUPTA, K. C., GARG, R., BAHL, I., BHARTIA, P. *Microstrip Lines and Slotlines*. 2nd ed. Artech House, 1996.
- [16] JILANI, M. T., WEN, W. P., ZAKARIYA, M. A., CHEONG, L. Y. Dielectric characterization of meat using enhanced coupled ring-resonator. In *IEEE Asia-Pacific Conference on Applied Electromagnetics*, 2014.
- [17] YOGI, R., GANGAL, S., AIYER, R., KAREKAR, R. Split modes in asymmetric microstrip ring resonator by flexible perturbation. *Microwave and Optical Technology Letters*, 1998, vol. 19, no. 2, p. 168–171.
- [18] SUMESH SOFIN, R. G., AIYER, R. C. Measurement of dielectric constant using a microwave microstrip ring resonator (MMRR) at 10 GHz irrespective of the type of overlay. *Microwave and Optical Technology Letters*, October 2005, vol. 47, no. 1, p. 11–14.
- [19] ABEGAONKAR, M. P., KAREKAR, R., AIYER, R. C. A microwave microstrip ring resonator as a moisture sensor for biomaterials: application to wheat grains. *Measurement Science and Technology*, 1999, vol. 10, no. 3, p. 195.
- [20] NAVARRO, J. A., CHANG, K. Varactor-tunable uniplanar ring resonators. *IEEE Transactions on Microwave Theory and Techniques*, 1993, vol. 41, no. 5, p. 760–766.
- [21] HSIEH, L. H., CHANG, K. Equivalent lumped elements G, L, C, and unloaded Q's of closed-and open-loop ring resonators. *IEEE*

- Transactions on Microwave Theory and Techniques*, 2002, vol. 50, no. 2, p. 453–460.
- [22] PUCCEL, R. A., MASSE, D. J., HARTWIG, C. P. Losses in microstrip. *IEEE Transactions on Microwave Theory and Techniques*, 1968, vol. 16, no. 6, p. 342–350.
- [23] HOPKINS, R., FREE, C. Equivalent circuit for the microstrip ring resonator suitable for broadband materials characterisation. *IET Microwaves, Antennas and Propagation*, 2008, vol. 2, no. 1, p. 66–73.
- [24] CHANG, K. MARTIN, S. WANG, KLEIN, J. L. On the study of microstrip ring and varactor-tuned ring circuits. *IEEE Transactions on Microwave Theory and Techniques*, 1987, vol. 35, no. 12, p. 1288–1295.
- [25] BRAY, J. R., ROY, L. Microwave characterization of a microstrip line using a two-port ring resonator with an improved lumped-element model. *IEEE Transactions on Microwave Theory and Techniques*, 2003, vol. 51, no. 5, p. 1540–1547.
- [26] BENEDEK, P., SILVESTER, P. Equivalent capacitances for microstrip gaps and steps. *IEEE Transactions on Microwave Theory and Techniques*, 1972, vol. 20, no. 11, p. 729–733.
- [27] GARG, R., BAHL, I. Microstrip discontinuities. *International Journal of Electronics*, 1978, vol. 45, no. 1, p. 81–87.
- [28] DAMEZ, J.-L., CLERJON, S., ABOUELKARAM, S., LEPETIT, J. Dielectric behavior of beef meat in the 1–1500 kHz range: Simulation with the Fricke/Cole–Cole model. *Meat Science*, 2007, vol. 77, no. 12, p. 512–519.
- [29] ELLAPPAN, P., SUNDARARAJAN, R. A simulation study of the electrical model of a biological cell. *Journal of Electrostatics*, 2005, vol. 63, p. 297–307.
- [30] YANG, Y., WANG, Z.-Y., DING, Q., HUANG, L., WANG, C., ZHU, D.-Z. Moisture content prediction of porcine meat by bioelectrical impedance spectroscopy. *Mathematical and Computer Modelling*, 2013, vol. 58, no. 3–4, p. 819–825.
- [31] SCHOENBACH, K. H., KATSUKI, S., STARK, R. H., BUESCHER, E. S., BEEBE, S. J. Bioelectrics - new applications for pulsed power technology. *IEEE Transactions on Plasma Science*, 2002, vol. 30, no. 1, p. 293–300.
- [32] DEAN, D., RAMANATHAN, T., MACHADO, D., SUNDARARAJAN, R. Electrical impedance spectroscopy study of biological tissues. *Journal of Electrostatics*, 2008, vol. 66, no. 3–4, p. 165 to 177.
- [33] JILANI, M. T., WEN, W. P., ZAKARIYA, M. A., CHEONG, L.Y. Determination of size-independent effective permittivity of an overlay material using microstrip ring resonator. *Microwave and Optical Technology Letters*, 2014 (accepted for publication).
- [34] GOUKER, M. A., KUSHNER, L. J. A microstrip phase-trim device using a dielectric overlay. *IEEE Transactions on Microwave Theory and Techniques*, 1994, vol. 42, no. 11, p. 2023–2026.

About Authors ...

Muhammad Taha JILANI received his Bachelor's degree in Electrical Engineering and Master's degree in Communication Technology from Muhammad Ali Jinnah University, Karachi, Pakistan, in 2007 and 2009, respectively. He is currently working towards his PhD degree in Electrical and Electronics Engineering at Universiti Teknologi Petronas, Malaysia. His research interests focus mainly on RF and microwaves spectroscopy for food quality applications.

Wong Peng WEN was born in Perak, Malaysia in 1984. He graduated from the University of Leeds with First Class BEng (Hons.) degree in Electrical and Electronic Engineering and completed his PhD degree in the same university in 2009. He has worked as a Senior Lecturer in Universiti Teknologi Petronas since 2010. His research interests include passive filters, tunable filters and filter miniaturization techniques.

Lee Yen CHEONG received the B.Sc. degree (First Class Hons.) in Mathematics and Physics from the University of Reading, and Ph.D. degree in Mathematics from the University of York, U.K., in 2006 and 2009, respectively. He is a corporate member of the Institute of Physics, U.K. He is currently a senior lecturer at the Dept. of Fundamental and Applied Sciences, Universiti Teknologi Petronas, Malaysia. His main research fields include all aspects of theoretical elementary particle physics and general relativity.

Mohammad Azman Bin ZAKARIYA received the B.Sc. degree in Electrical Engineering from Universiti Teknologi Malaysia, and the M.Sc. degree in Communications and Signal Processing, both from the University of Newcastle upon Tyne, UK. He is a Lecturer at Universiti Teknologi Petronas, Malaysia, and is working towards his PhD at Universiti Sains Malaysia. His research interests include dielectric resonator antennas & defected ground structures.

Muhammad Zaka Ur REHMAN received the B.S. degree in Electronics from COMSATS Inst. of Information Technology, Islamabad, Pakistan in 2007, the MSc. degree in DSP in Communication Systems from Lancaster University, UK, in 2010, and is currently working toward the PhD degree in Electrical Engineering at the Universiti Teknologi Petronas, Perak, Malaysia. His research interests include RF MEMS for microwave applications, substrate integrated waveguide structures and reconfigurable filters design.